Structural Characterization of Oxide Materials by the Anomalous X-ray Scattering Method

Yoshio WASEDA* and Kazumasa SUGIYAMA*

The fundamentals of the anomalous X-ray scattering (AXS) method and its potential power have been described with some selected examples by making available the local chemical environment around a specific element as a function of radial distance in multi-component oxide materials. The usefulness of this relatively new method using the anomalous dispersion effect of X-rays was also given by the results of surface structural analysis of nanometer-sized zinc ferrite particles.

1. INTRODUCTION

There is a vast amount of research on new materials going on today and a clear understanding of the physical and chemical properties of these new materials is known to depend heavily upon their structural characterization at a microscopic level. The development of disordered materials such as amorphous metallic alloys and oxide glasses stimulates current interest in this rapidly growing field, because they show some interesting electronic, magnetic, mechanical and chemical properties. In contrast to crystalline materials, the atomic arrangement in disordered materials is not periodic and the novelty of their properties should be attributed to this particular non-periodicity.

The near neighbor atomic correlations of the individual chemical constituents or the local chemical environments around a specific element is essentially required for describing the quantitative structure in multi-component systems of interest. For this purpose, several techniques have been employed and the Anomalous X-ray Scattering (hereafter to be referred to as AXS) method by applying the so-called anomalous dispersion effect near the absorption edge of a constituent element has recently received much attention, because the availability of synchrotron radiation source has greatly improved both acquisition and quality of the AXS data over those obtainable using conventional X-ray source.[1,2]

The main purpose of this paper is to present an extended introductory treatise on the novel application of AXS method to structural characterization of oxide materials.

---

* 早稲田嘉夫, 杉山和正 : Institute for Advanced Materials Processing, Tohoku University, Sendai 980-77, Japan.

2. FUNDAMENTALS OF THE AXS METHOD

When the incident energy of X-rays is tuned to the close vicinity of the K- or L-shell absorption edge of a constituent, the scattering intensity shows the distinct energy dependence due to the anomalous dispersion effect. Physically, this can be attributed to the resonance effect in which the oscillations of the corresponding K- or L-shell electrons closely connected to the scattering of X-rays are strongly disturbed.[3]

In the vicinity of the absorption edge, where the anomalous dispersion effect is notable, the atomic scattering factor f in practice should be used in the following form.

$$f(Q, E) = f^0(Q) + f'(E) + if''(E) \tag{1}$$

where Q is the wave vector given by $4\pi \sin\theta/\lambda$, θ is a half of the scattering angle and λ is the wavelength. The f^0 term is the normal atomic scattering factor for radiation at energy far from any absorption edge. f' and f'' are the real and imaginary components of the anomalous dispersion, respectively. These dispersion terms strictly depend upon both the energy E and the wave vector Q. However, in practice, the Q-dependence appears insignificant.[3] Thus, the variation of f' and f'' with Q is generally ignored in Eq. (1).

The typical features of the energy dependence of f' and f'' is illustrated in Fig. 1 using iron as
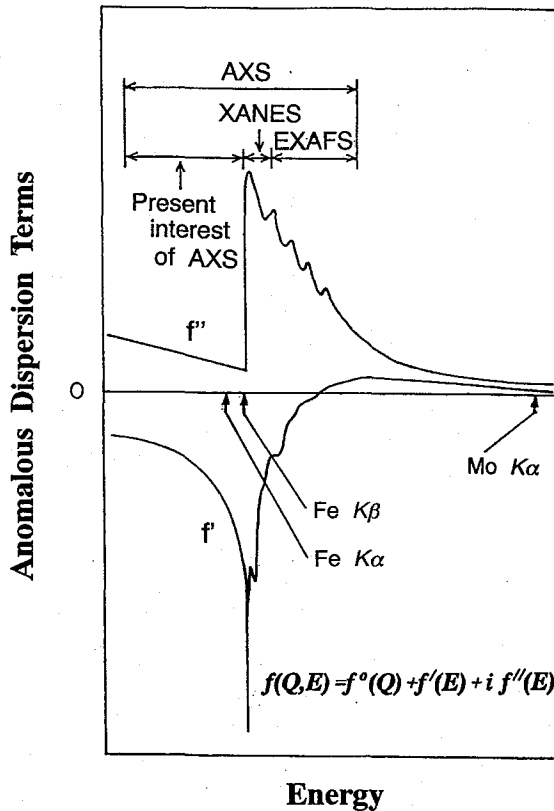

Fig. 1. Schematic diagram for anomalous dispersion factors of iron near the Fe K-absorption edge.

an example. The component of f' exists on either side of the absorption edge and the monotonic energy dependence is detected in the lower energy side, although the oscillations at higher energy side are observed due to the particular near edge phenomena such as XANES and EXAFS.[4,5] Such oscillatory profile of f' and the significant fluorescent radiation at the higher energy side of the edge frequently prevent us from obtaining sufficiently reliable structural information. Thus the lower energy side of the absorption edge is usually employed for structural characterization of materials by the AXS method. It is also noted that the anomalous dispersion factors experimentally determined[6,7] show a reasonable agreement with the theoretical values by the Cromer-Liberman scheme[8] which is probably the best method for a wide energy region.

Since the characteristic absorption edges of various elements are separated by, at least, several hundred eV, the change in scattering intensity can be made with sufficient atomic sensitivity by the anomalous dispersion effect arising from the energy variation of about $200 \sim 300$ eV, even for two elements of nearly the same atomic number. For example, the combination of Fe $K\beta$ radiation with Mo $K\alpha$ or Fe $K\alpha$ radiation enables us to provide a detectable difference in scattering intensity from an iron and nickel mixture. The radiation with an energy of 7.11 keV, closer to the absorption edge of the iron atom, can offer more advantage by increasing an appreciable difference in the atomic scattering factor.

Let us consider AXS measurements in the lower energy side of the absorption edge of a certain constituent, for example the element A. Since the imaginary component of f'' is quite small and almost constant at this energy region, the detected variation in intensity can be attributed to only to the change of the real component of f' for the element A. Then, the following equation providing the reduced environmental interference function for the element A is readily obtained for a multi-component systems;[9]

$$\Delta i(Q) = \frac{(I_{E1}(Q) - \langle f_{E1}^2 \rangle) - (I_{E2}(Q) - \langle f_{E2}^2 \rangle)}{c_A(f'_{AE1} - f'_{AE2})W(Q)}$$
$$= \int_0^\infty 4\pi r^2 \sum_{J=1}^m \frac{Re[f_{jE1}(Q) + f_{jE2}(Q)]}{W(Q)}(\rho_{Aj} - \rho_{0j})\frac{\sin(Qr)}{Qr}dr \qquad (2)$$

with

$$W(Q) = \sum_{J=1}^m c_j Re(f_{jE1}(Q) + f_{jE2}(Q)) \qquad (3)$$

where $I(Q)$ the coherent scattering intensity in electron unit per atom (absolute intensity), c_j and f_j the atomic fraction and X-ray atomic scattering factor of element j, respectively. m is the number of the elements in the system, ρ_{Aj} the number density function of element j around element A, and ρ_{0j} the average number density for the element j. "Re" indicates the real part of the value in the parentheses. The subscripts $E1$ and $E1$ represent the incident energies. The summation in the above equation indicates the sum over the constituents of a sample. The environmental RDF for the element A can be determined by Fourier transformation of the environmental interference function, $Q\Delta i(Q)$;

$$4\pi r^2 \rho_A(r) = 4\pi r^2 \rho_0 + \frac{2r}{\pi}\int_0^\infty Q\Delta i(Q)\sin QrdQ \qquad (4)$$

These equations suggest that an environmental structure around a specific element can be estimated by measuring the energy dependence of the scattering intensity near the absorption

edge of a chosen element without complete separation into individual partial structural functions.[2] This method is frequently referred to as the energy derivative technique.

Even if the incident energy for AXS measurements is set below the absorption edge, some fluorescent radiations, which mainly originate form the tail of the band pass and the higher harmonic diffraction of the monochromator crystal, are sometimes significantly detected. It should be noted that the correction of such a fluorescent component form the observed AXS intensity is crucial in order to get sufficiently reliable data. The principle of the correction procedure for a fluorescent component is as follows. The energy resolution of a solid state detector is sufficient to separate $K\alpha$ component from the scattered photons. On the other hand, the $K\beta$ component overlapping with the scattered photons can be numerically subtracted in the data reduction process coupled with the measured intensity of $K\alpha$ during the course of the experiment and the intensity ratio of $K\beta/K\alpha$.[10] It may be noticed that such ratio is almost independent of the excitation energy as theoretically predicted.

3. SELECTED EXAMPLES OF STRUCTURAL STUDY OF DISORDERED MATERIALS

Germanate (GeO_2) glass is believed to have an atomic structure similar to a silicate (SiO_2) glass, although there have been rather little structural investigations. Therefore, the AXS method was applied to the GeO_2 glass at the Ge K-absorption edge. The environmental structure around Ge was carefully determined and also compared to the conventional X-ray diffraction results with Mo $K\alpha$ radiation. This measurement is also oriented towards the understanding of the usefulness of the AXS method.

Fig. 2 shows the intensity profiles of GeO_2 glass measured at two energies of 10.805 and 11.080 keV below the Ge K-absorption edge (11.103 keV) and their difference is given at the top of this figure.[11] Intensities of the second and third peaks relative to the first peak increase in the
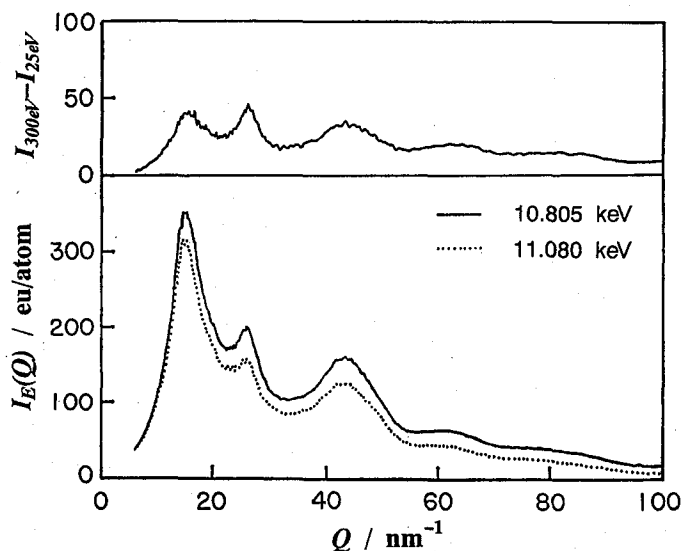

Fig. 2. Differential intensity profile of GeO_2 glass (top) obtained from the intensity data set (bottom) measured at energies of 10.805 (solid) and 11.080 (dotted) keV.[11]
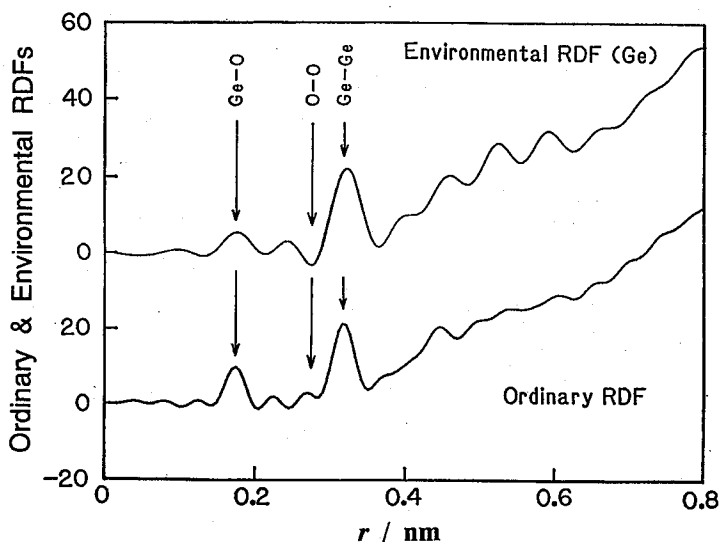
Fig. 3. Environmental RDF for Ge (top) and ordinary RDF (bottom) of GeO$_2$ glass.[11]

differential profile.   Taking account of the fact that the atomic correlations around a Ge atom are emphasized in the differential curve, we can imagine that the second and third peaks are more strongly attributed to the local atomic configurations around Ge than the first peak.   The environmental radial distribution function (RDF) for Ge estimated using Eq. (4) is illustrated in Fig.3 together with the ordinary RDF.   Comparing these two profiles, it is readily found that the peak caused by the O-O pairs is disappears in the environmental RDF for Ge.   This strongly supports that the present AXS measurements work well.   The distances and coordination numbers obtained in this AXS measurement clearly indicate that each Ge is surrounded by four oxygens with a Ge-O distance of 0.175 nm.   Thus, it is reasonably said that the GeO$_4$ tetrahedron is a fundamental local unit structure in germanate glass.   The number of Ge around Ge is four and the six coordination of O-O pairs is obtained form the ordinary RDF data.   Then, each oxygen located at the corner of the tetrahedron is likely to be bonded with two Ge, so that the network structure formed by the tetrahedra joined at their corners is quite feasible.

Using the Ge-Ge and Ge-O distances in the present work, the Ge-O-Ge bond angle is estimated to be about 132°. Incidentally the bond angle in the α-quartz-type GeO$_2$ crystal is 130°.   Therefore, it is imagined that packing of the GeO$_4$ tetrahedra might be similar to that found in the crystalline modification of GeO$_2$ as seen in the structural model of SiO$_2$ glass.[12]

The binary GeO$_2$-P$_2$O$_5$ glass system is interesting, because of a change in environment around Ge with increasing P$_2$O$_5$ content.   There have been some conflicting results[13-16] and such disagreement may be due to the difficulty in determining the structural information of Ge-O pairs in this binary system using the spectroscopic data alone.   Then, the environmental structural information around Ge, namely whether Ge atoms prefer tetrahedral sites coordinated by four oxygen atoms or octahedral sites by six oxygen atoms, is strongly required.   This promopted us to use the AXS method.[17]

The interference functions $Qi(Q)$ of three GeO$_2$-P$_2$O$_5$ glass samples obtained by Mo $K\alpha$

radiation are shown in Fig. 4. The ordinary RDFs calculated from these interference functions are illustrated in Fig. 5. It may be suggested that the ordinary RDFs contain six partial correlations of Ge-O, P-O, Ge-P, O-O, Ge-Ge and P-P pairs. From the ionic radius of the
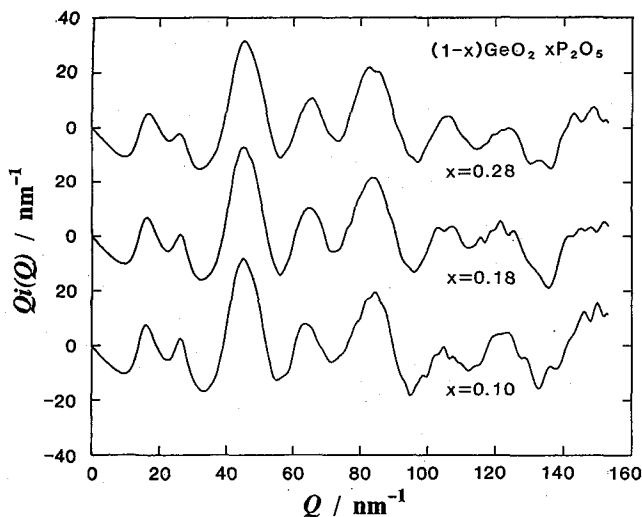
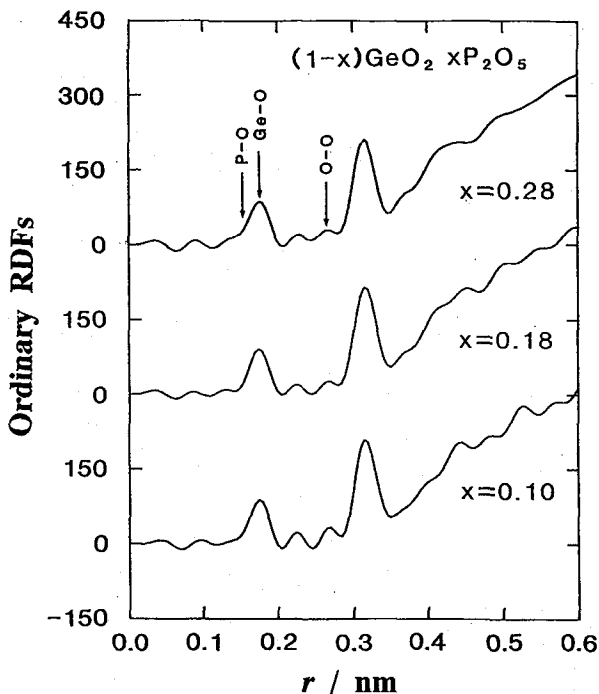Fig. 4. The interference functions $Qi(Q)$ of the GeO_2-P_2O_5 glasses obtained by Mo $K\alpha$ radiation.[17]

Fig. 5. The ordinary RDFs of the GeO_2-P_2O_5 glasses, calculated from the interference function of Fig. 4.[17]

constituent elements, the first peak around 0.18 nm may be allocated to the mixed correlations of the Ge-O and P-O pairs. However, the distances of tetrahedrally coordinated P-O (0.150 nm) and Ge-O (0.175 nm) pairs are so close that the ordinary RDF analysis is difficult to separate the information of these two atomic pairs. Then, the use of the AXS method reduces such difficulty by providing the environmental structure around a specific element.
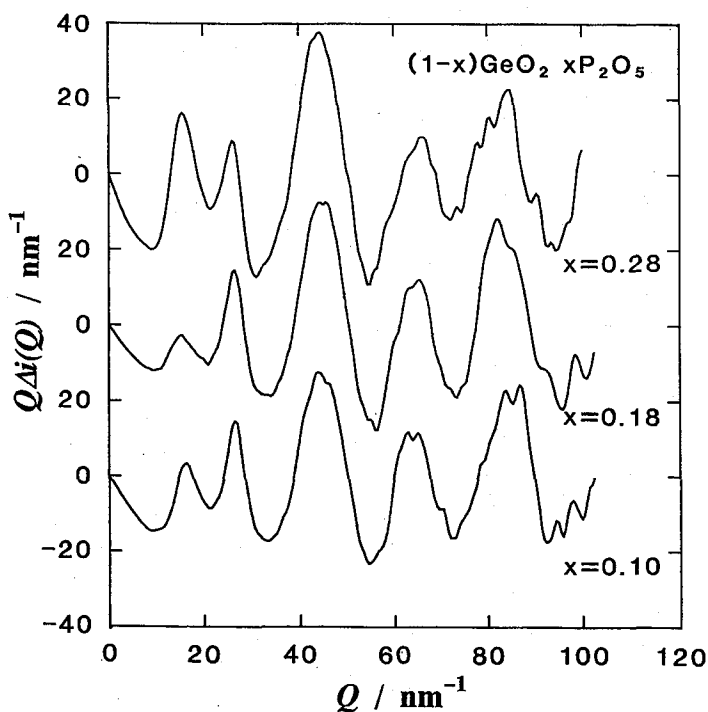

Fig. 6. Environmental interference functions $Q\Delta i(Q)$ for Ge of the GeO$_2$-P$_2$O$_5$ glasses.[17]

The scattering intensity profiles of each sample were measured at two energies near the Ge K-absorption edge in order to obtain the environmental (differential) interference functions $Q\Delta i(Q)$ and their RDFs, and the results are shown in Figs. 6 and 7, respectively. The environmental functions contain only three partial information on Ge-O ,Ge-P and Ge-Ge pairs. For this reason, the first peak at about 0.18 nm in the environmental RDFs is the Ge-O correlation because the P-O correlations are not included. The peaks around 0.24 nm are considered to be due to statistical fluctuations and enhancements of the Ge-O and Ge-Ge pair correlations. For convenience, the calculated values for Ge-O and Ge-Ge pairs are given by dotted lines using the case of 0.90GeO$_2$0.10P$_2$O$_5$ glass as an example. The coordination number of Ge-O pairs can be estimated from the corresponding peak area with the assumption that the peak shape is Gaussian. The results are summarized in Table 1 together with the information of pure GeO$_2$ glass.[11]

The distance of the Ge-O pairs and the coordination number of oxygen atoms clearly increase with P$_2$O$_5$ content. These AXS data are consistent with the results obtained by
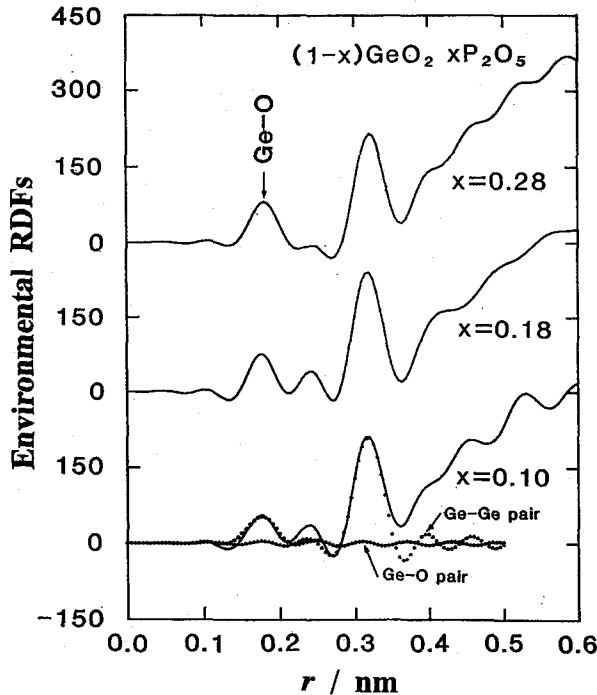
Fig. 7. Environmental RDFs of the GeO_2-P_2O_5 glasses. Dotted lines of $0.90GeO_2 0.10P_2O_5$ glass are an example of calculation using correlations of Ge-O and Ge-Ge pairs.[17]

Table 1. Comparison of the distance (r) and coordiantion number (N) for the Ge-O pairs of three GeO_2-P_2O_5 glasses determined by the AXS method.[17]

Chemical composition	AXS measurement Ge-O		Density (Mg/m^3)
	r (nm)	N (atom)	
GeO_2	0.175	4.1	3.64
$0.90GeO_2 \cdot 0.10P_2O_5$	0.175	3.9	3.61
$0.82GeO_2 \cdot 0.18P_2O_5$	0.177	5.1	3.59
$0.72GeO_2 \cdot 0.28P_2O_5$	0.182	5.3	3.55

r: ±0.002, N: ±0.4

infrared absorption[13] and Raman spectroscopy[14] and the variations of the molar refractivity, molar volume and thermal expansion coefficient.[13] Therefore, we can interpret the increase in the oxygen coordination number around Ge is attributed to the mixed state of the octahedral and tetrahedral coordinations of Ge in GeO_2-P_2O_5 glass system. A detailed structural model of GeO_2-P_2O_5 glass has not been established yet. Nevertheless the present AXS analysis suggests the change of the coordinated oxygen atoms around Ge in this glass system induced by the addition of the P_2O_5 component.

Refinement of the structural parameters in near neighbor region, in addition to the nearest-neighbor correlation, is quite useful for further discussion of the atomic scale structure of
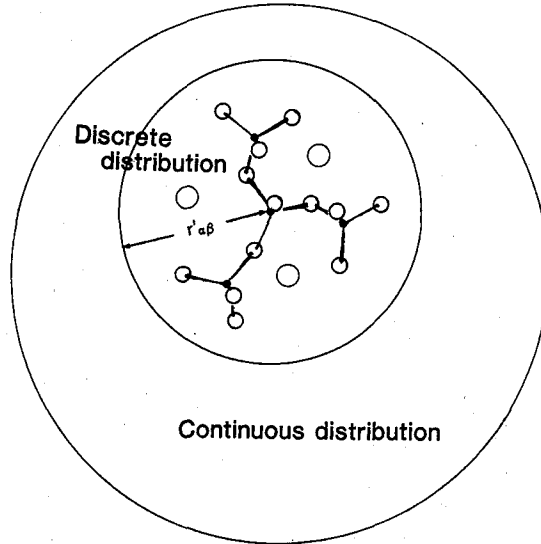
Fig. 8. Schematic representation for the structural model of a disordered oxide system.

disordered materials. For this purpose, the least-squares variational method proposed by Narten[18] enables us to provide one way when applying to both the ordinary interference function $Qi(Q)$ and the environmental interference function $Q\Delta i(Q)$. The essential idea of Narten's approach is based on the characteristic structural features of oxide glasses and melts exemplified by the contrast between the narrow distribution of local ordering in the shorter distance region and a complete loss of positional correlations in the longer distance one. In other words, the average number of element k around an element i, N_{ik} is separated by an average distance, r_{ik} and its distribution may be described by a discrete Gaussian like distribution with a mean-square variation of $2b_{ik}$. On the other hand, the distribution for higher order correlations is approximately expressed by a continuous distribution with an average number density of a system. Schematic structural description for this case is given in Fig. 8. These concepts may be represented using the following equation with respect to the interference function.

$$Qi(Q) = \sum_{j=1}^{m} \sum_{k} c_j \frac{f_j f_k}{\langle f \rangle^2} \frac{N_{jk}}{r_{jk}} \exp(-b_{jk}Q^2) \sin(Qr_{jk})$$
$$+ \sum_{\alpha=1}^{m} \sum_{\beta=1}^{m} c_\alpha c_\beta \frac{f_\alpha f_\beta}{\langle f \rangle^2} \exp(-b'_{\alpha\beta}Q^2) 4\pi\rho_0 \frac{Qr'_{\alpha\beta}\cos(Qr'_{\alpha\beta}) - \sin(Qr'_{\alpha\beta})}{Q^2} \qquad (5)$$

The quantities of $r'_{\alpha\beta}$ and $b'_{\alpha\beta}$ correspond to the mean and the variance of the boundary region which need not be sharp.[18,19] It may be noted that the first and second terms of Eq. (5) represent the discrete Gaussian-like distributions and a continuous distribution with an average number density in the higher order correlations, respectively. In practice, the structural parameters are determined by estimating the interference function using the least-squares calculation of Eq. (5) so as to reproduce the experimental interference function. The environmental interference function can also be readily calculated by taking the difference of the calculated ordinary coherent scattering intensity similarly estimated at the two energies in the AXS measurements and compared with the experimental AXS data. Thus, it would rather be
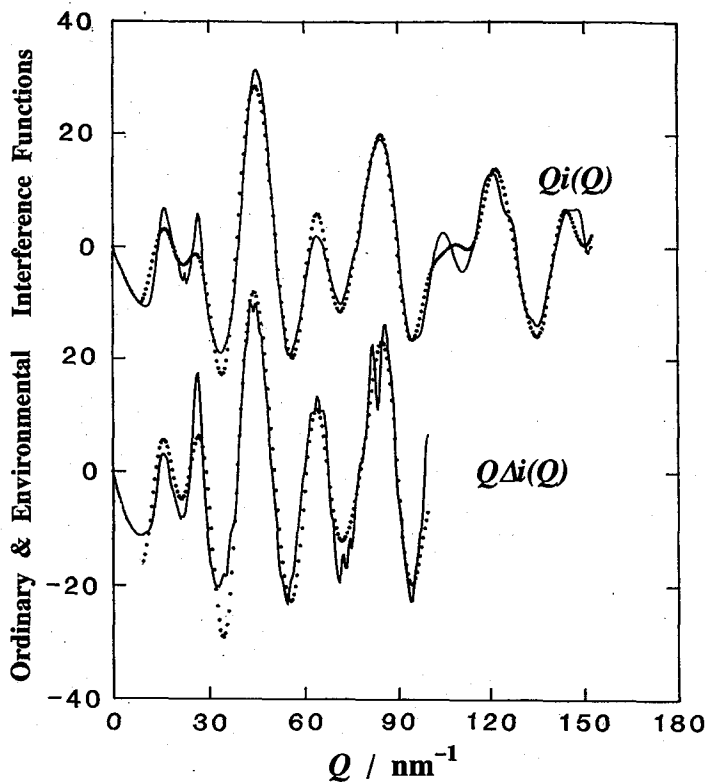
Fig. 9. Comparison of the calculated interference functions with the experimental data for GeO$_2$ glass using the least-squares variational method.[20]

Table 2. Structural parameters of the near neighbor corrlations for GeO$_2$ glass and α-quartz-type GeO$_2$ crystal.[20]

Density (Mg/m^3) Pairs	Glassy GeO$_2$ 3.64		α-quartz-type GeO$_2$ 4.21	
	r (nm)	N (atom)	r (nm)	N (atom)
Ge-O	0.173	4.1	0.174	4.0
Ge-O	0.365	4.1	0.348	6.0
Ge-O	0.411	9.8	0.428	14.0
Ge-O	0.488	3.4*	0.479	4.0
Ge-O	0.541	6.0*	0.540	7.0
Ge-Ge	0.317	4.1	0.315	4.0
Ge-Ge	0.453	3.9	0.447	6.0
Ge-Ge	0.497	4.0	0.499	6.0
Ge-Ge	0.535	5.1*	0.539	6.0
O-O	0.277	6.4	0.284	6.0
O-O	0.330	5.1*	0.337	6.0
O-O	0.434	3.4*	0.412	4.0
O-O	0.495	13.6*	0.507	16.0

*) fixed

stressed here, that the resolution of the structural parameters can be improved at the reasonable level by the least-squares variational method when applying to not only $Qi(Q)$ but also $Q\Delta i(Q)$.

Figure 9 shows a comparison of the calculated interference functions with the experimental data using the case of GeO_2 glass and the resultant structural parameters are summarized in Table 2 together with the values of α-quartz-type GeO_2 crystal.[20] These experimental results again supports that packing of the GeO_4 tetrahedra is very similar to that found in the modification of GeO_2 crystal structure, as has been suggested for SiO_2 glass.[12] It would be interesting to give an another example obtained by this method.

A number of interesting materials have been prepared by sol-gel method. Zirconium oxide is included in this category and the thermal decomposition of amorphous ZrO_2 formed from zirconium alkoxides[21,22] and zirconium salts[23,24] are known to produce a metastable tetragonal ZrO_2 (t-ZrO_2), in addition to monoclinic ZrO_2 (m-ZrO_2) which is actually stable under about 1,273 K. However, the formation of t-ZrO_2 at low temperature is not revealed yet. For example, Cypres et al.[25] and other two research groups[26,27] proposed that the stabilization of t-ZrO_2 is attributed to various anionic impurities such as OH^-, whereas Garvie[23] and some other persons[21,28] suggested that it should be rather related to the particle size effect. The stabi-
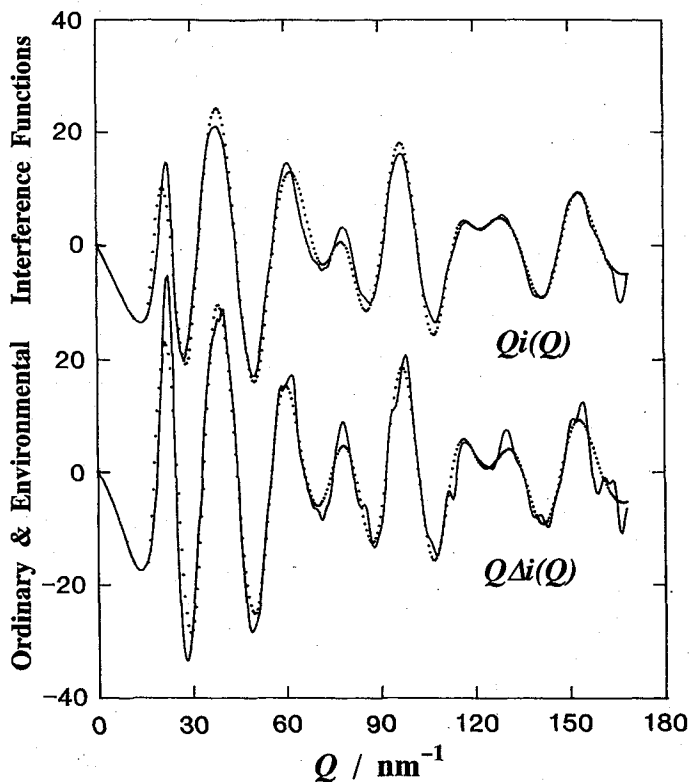

Fig. 10. (Top) Interference function $Qi(Q)$ of amorphous ZrO_2 obtained from the intensity measurement at the energy of 17.698 keV. (Bottom) Environmental interference functions $Q\Delta i(Q)$ for zirconium of amorphous ZrO_2 obtained from the intensity data measured at the Zr K-absorption edge.[30]

lization of t-ZrO$_2$ may be explained by the similarity of local ordering structure between amorphous and t-ZrO$_2$.[28,29] This implies that the structure of amorphous ZrO$_2$ holds the key to give the conclusive remark regarding its particular crystallization behavior by low temperature heating. Recently, the AXS method has been applied to obtain the atomic structure of hydrolytic condensed zirconium oxide at longer distance as well as the structure in the nearest-neighbor region including the structural similarity between amorphous ZrO$_2$ and crystalline ZrO$_2$.[30] The results are as follows.

Two scattering intensity profiles were measured at the energies close to the Zr K-absorption edge and the resultant environmental interference function $Q\Delta i(Q)$ of hydrolytic condensed zirconium oxide is given in Fig. 10. The ordinary interference function $Qi(Q)$ estimated from the diffraction data of single energy of 17.698 keV is also illustrated in this figure for comparison.

The profiles of these interference functions consist of the first peak at about 22 nm^{-1} followed by a number of peaks, which indicate a considerable fraction of local ordering unit structures exist in this glass structures although their distribution appears to be no long range ordering. These features contrast to the case of metallic glasses, where the rapid damping of interference function is clearly observed. The environmental and ordinary RDFs calculated from the interference functions are shown in Fig. 11.

The ordinary RDF corresponds to the sum of three partial RDFs of Zr-O,Zr-Zr and O-O. From the information of ionic radii of the constituent elements, the first peak around 0.22 nm and 0.34 nm can be suggested to be Zr-O and Zr-Zr pairs, respectively. It is worth mentioning in
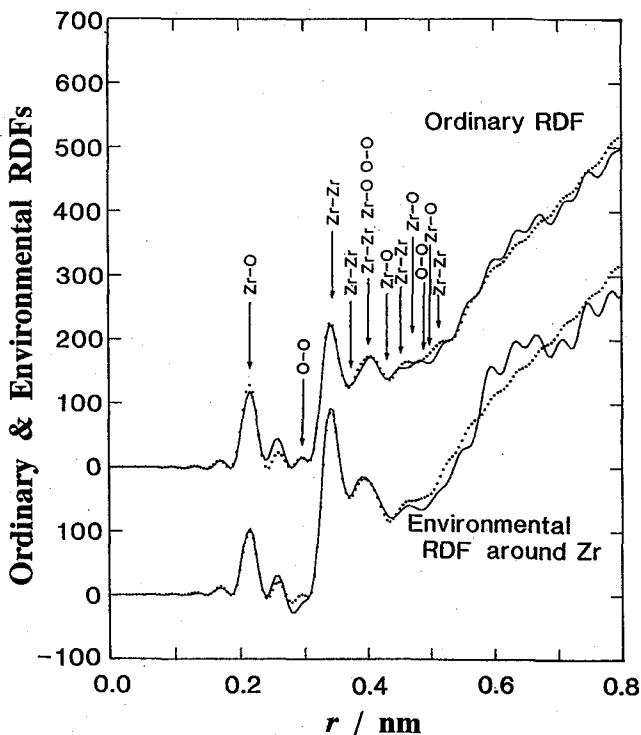

Fig. 11. Ordinary and environmental RDFs calculated from the interference functions of Fig. 10[30].

the ordinary RDF that the Zr-Zr pair around 0.34 nm is well coincident with the atomic pairs characterized by the m-ZrO_2 structure. Therefore, the fundamental local structure of the present amorphous ZrO_2 sample seems to be rather closer to that of m-ZrO_2 than t-ZrO_2. Structural parameters of Zr-O and Zr-Zr pairs are likely to be obtained. However, the definite and precise information of the local atomic arrangements of amorphous ZrO_2 cannot be determined as a unique solution from the present ordinary RDF data alone. This is particularly true in the higher order correlations, because more than two kinds of atomic pairs usually overlap at longer distances.

As shown in Fig. 11, the structural features observed in the environmental RDF for Zr is essentially similar to those of ordinary RDF of amorphous ZrO_2, although the environmental RDF includes only the atomic correlations of Zr-O and Zr-Zr pairs. This is mainly due to the reason that the contribution of O-O pairs to the ordinary RDF is not so significant. Nevertheless, it is noticed that the correlation of Zr-Zr pairs in the environmental RDF is rather distinct at the distance of 0.34 nm, compared with that of the ordinary RDF. When such valuable different nature observed in the environmental RDF determined by the AXS measurements is coupled with the ordinary RDF data, the resolution of the structural parameters for Zr-O and Zr-Zr pairs can be improved even in the higher order correlations when using the least-squares variational method.

The present analysis qualitatively suggests that the structural features of amorphous ZrO_2 are rather close to those of m-ZrO_2 than t-ZrO_2 structure. Then, at the first step, the 22% random vacancy m-ZrO_2 structure model based on the density measurements was applied for explaining the experimental RDF data. However, the converged structural parameters could not reproduce the experimental RDFs, particularly the RDF data in the distance of 0.37 nm,

Table 3. Structural parameters of the near neighbor correlations for amorphous ZrO_2.[30]

Density (Mg/m³) Pairs	Amorphous 4.47		Monoclinic 5.74		Tetragonal 5.86	
	r (nm)	N (atom)	r (nm)	N (atom)	r (nm)	N (atom)
Zr-O	0.214	5.8	0.216	7.0	0.226	8.0
Zr-O	0.395	2.3	0.385	8.0		
Zr-O	0.427	5.4	0.444	12.0	0.413	12.0
Zr-O	0.465	6.3			0.448	12.0
Zr-O	0.495	4.1	0.490	8.0		
Zr-Zr	0.341	4.4	0.347	7.0		
Zr-Zr	0.371	1.6			0.366	12.0
Zr-Zr	0.398	2.5	0.415	3.0		
Zr-Zr	0.449	1.4	0.456	1.0		
Zr-Zr	0.509	2.1	0.524	6.0	0.519	6.0
O-O					0.265	6.0
O-O	0.296	7.4*	0.285	9.5		
O-O					0.344	8.0
O-O	0.398	7.4*	0.394	9.5		
O-O					0.439	12.0
O-O	0.486	4.3*	0.474	5.5		

*) fixed

which corresponds to the first Zr-Zr pairs in t-ZrO_2 structure. It should also be kept in mind that the atomic configurations of amorphous ZrO_2 are not exactly identical to those of m-ZrO_2. Then, the random vacancy model coupled with both t-ZrO_2 and m-ZrO_2 structures was employed at the second step as initial parameters. After several iterations, the converged interference functions drawn with dotted lines in Fig. 10 were obtained. The resultant structural parameters are summarized in Table 3 together with the crystalline zirconium oxides.[31,32] For convenience, the interatomic distances obtained by the present analysis are given by the arrows in Fig. 11.[31] Since that the variations of r and N depend upon the initial structural model, the parameters in Table 3 should be read as not unique but possible solution with respect to the structure of amorphous ZrO_2.
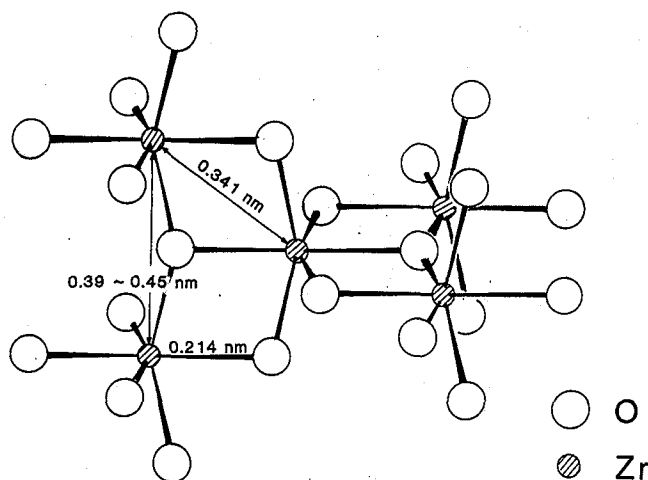

Fig. 12. Schematic diagrams of the atomic structure of amorphous $ZrO_{.2}$ [30]

The present results quantitatively indicate that the fundamental local ordering unit of amorphous ZrO_2 is octahedrally coordinated zirconium and its distance is 0.214 nm. About the first neighboring Zr-Zr pairs, a zirconium is surrounded by about four zirconiums at about 0.34 nm forming a particular structural unit. With these facts, a three-dimensional structural model illustrated in Fig. 12 is proposed as one of the possible amorphous structures by considering the simple geometrical factors. This model indicates that the zirconium octahedra link each other with sharing four edges of coordination polyhedra.

The present results also indicate that the progress of the hydrolysis condensation process makes the structure of monomeric alkoxide more dense, so as to increase of the shared edge number of coordination polyhedra and that calculated shared edge length in both structural model of about 0.26 nm is rather shorter than the estimated edge length of the regular zirconium octahedron. Consequently, the very distorted feature of zirconium octahedra is suggested in the structure of amorphous ZrO_2. Murase et al.[24] reported that the crystallization behavior of amorphous ZrO_2 produced by sol-gel method strongly depends on the conditions of sample preparation. Therefore, it is rather difficult to determine which mechanism is actually significant in the formation of t-ZrO_2 from amorphous ZrO_2. Nevertheless, the present results, at least, provide that it is quite unrealistic to identify the local ordering structure of amorphous ZrO_2 to be responsible for the formation of t-ZrO_2 as frequently discussed in the previous works.
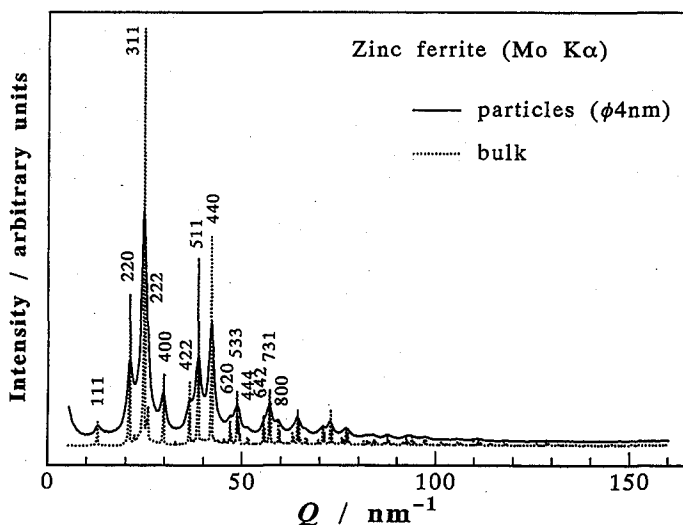
Fig. 13. Comparison of scattering intensities of 4 nm zinc ferrite particles and the bulk sample.[34]

4. SURFACE STRUCTURAL ANALYSIS OF NANOMETER-SIZED PARTICLES

Various reactions occur on the surface of materials and then there is an increasing need for the information of surface structure. On the other hand, nanometer-sized particles appear to indicate some peculiar features distinct from those in the bulk, because of the large fraction of the surface atoms. For example, the nanometer-sized zinc ferrite particles show an extremely large magnetization compared to the value reported for the bulk.[33] In order to explain such characteristic property, the atomic structure of their surface is strongly required. The AXS method is one way to obtain the information of surface structure of nanometei-sized particles.

The scattering intensity profile for zinc ferrite (crystal-line) particles with an average size of 4 nm is compared with that of the bulk in Fig. 13.[34] A scattering intensity from nanometer-sized particles is extremely broadened because of their small particle size.

The scattering intensity for crystalline particles with a certain size may be calculated using the following simple equation based on Warren's approach :[35]

$$I(Q) = \sum_{j=1}^{N} \sum_{k=1}^{N} f_j f_k \exp(-2M) \frac{\sin(Qr_{jk})}{Qr_{jk}} \tag{6}$$

where N is the total number of atoms in a crystalline particle, f_j the X-ray atomic scattering factor of the element j and M the Debye-Waller temperature factor. The Debye-Waller factor of zinc ferrite particles were computed from the Debye temperature (630 K), which was estimated from those of ZnO (600 K) and Fe_2O_3 (660 K). It would be mentioned here, that the contribution of the interparticle interference was excluded in this calculation, because it has been shown to give a significant contribution only in the small angle region.[36]

A scattering intensity calculated form inner atoms of the 4 nm zinc ferrite particles is compared with the experimental intensity data in Fig. 14. The disagreement is clearly detected. It may be added that the calculated peak intensities become closer to the experimental ones when choosing a smaller average particle size. However, the relatively large background intensity
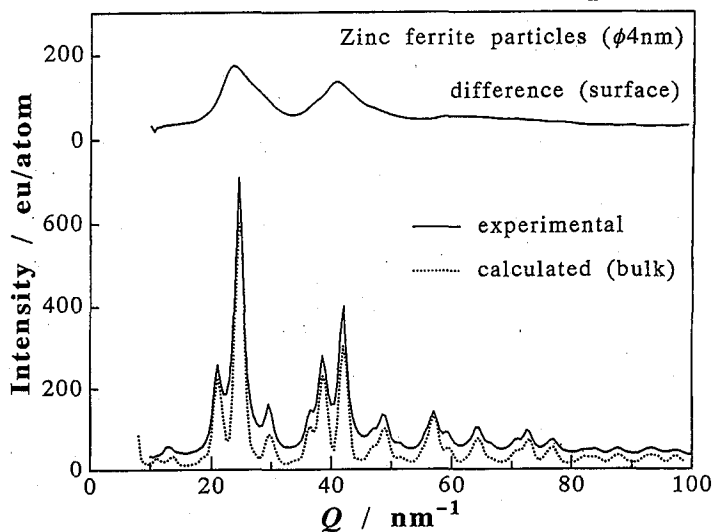
Fig. 14. Comparison of the observed intensity with the intensity calculated from particles without considering surface atoms.[34]

cannot be reproduced by simply changing the particle size. Thus, another model is required for explaining the experimental data of nanometer-sized zinc ferrite particles.

The difference between two scattering intensities of calculation and experiment, is given in the top of Fig. 14 and it represents scattering intensity from monolayer surface atoms of these particles.

This difference profile shows an amorphous-like intensity pattern consisting of the broad first peak at about 25 nm^{-1} and the second and third broader and weaker peaks at about 40 and 65 nm^{-1}. Similarity to the amorphous zinc ferrite[37] is readily confirmed in the results of Fig. 15

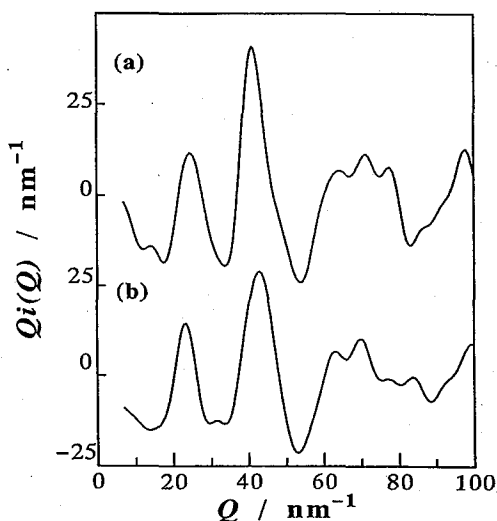
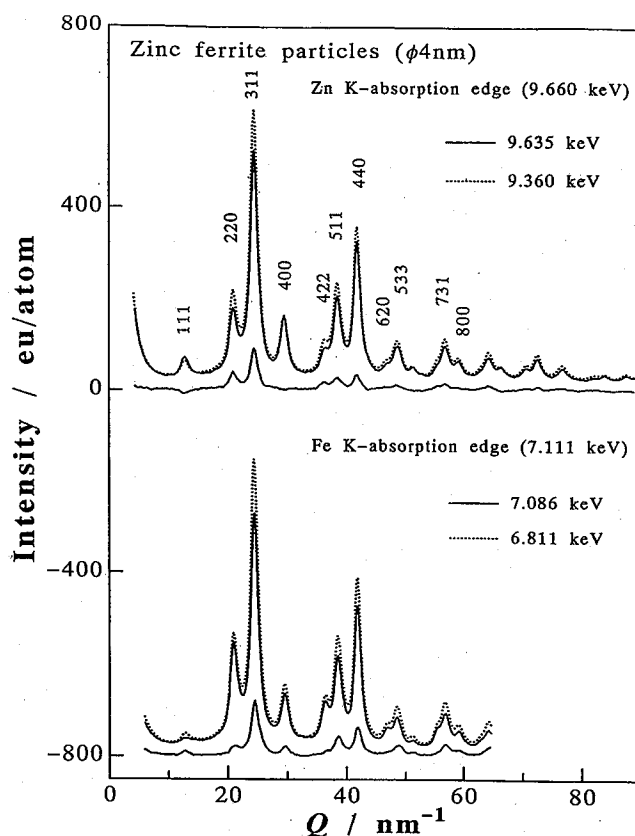Fig. 15. Interference functions of (a) monolayer surface atoms and (b) amorphous zinc ferrite film.[34,37]

Fig. 16. AXS profiles of 4 nm zinc ferrite particles at Zn and Fe K-absorption edges.[34]

representing by the interference function form, although there are difference in detail. This suggests that monolayer surface atoms form rather an amorphous-like atomic structure than the zinc ferrite crystalline structure inside the particle.

In order to check this point, the AXS measurements were recently made at the Fe and Zn K-absorption edges[34] and the results are shown in Fig. 16. The details of the structure of the surface atoms in zinc ferrite particles cannot be revealed yet, so that the total scattering intensity in Fig. 13 and the AXS intensities in Fig. 16 were calculated by substituting the scattering intensity of the amorphous zinc ferrite for the intensity due to the surface atoms. This corresponds to the assumption that atoms at the surface are randomly displaced against atoms inside the particle and then the average phase shift between atoms at the surface and inside the particle in every direction around the particle becomes zero. The calculated intensities are compared with the experimental data in Fig. 17. Although the boundary between the surface and bulk components is sharp in the present model, a gradual change from the glass-like structure to the crystal might be more plausible. Nevertheless, it may not be overemphasized that good agreement is found including the back-ground intensities as well as for the peak intensities in three cases. For this reason, the presence of the amorphous-like structure on the surface is considered to be, at least in a sense of the necessary condition, at best for explaining the scattering
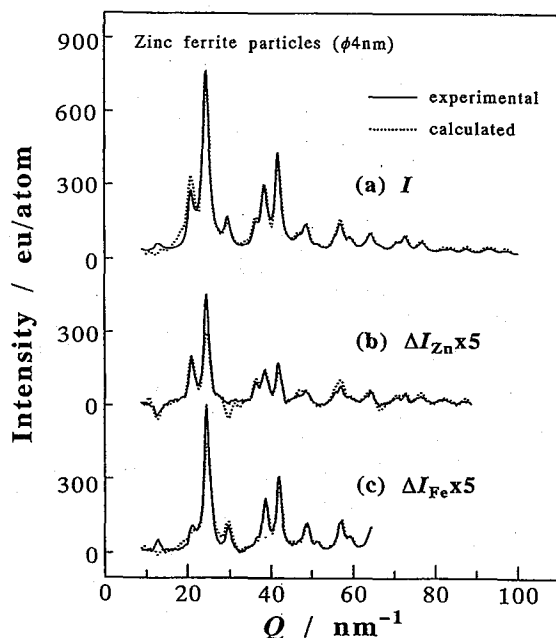
Fig. 17. The observed and calculated intensities (a) obtained by the ordinary
X-ray diffraction and differential intensities obtained by the AXS
measurements below (b) Zn and (c) Fe K-absorption edges.[34]

intensities for the nanometer-sized zinc ferrite particles by reproducing the three independent scattering intensity profiles as shown in Fig. 17.

5. CONCLUDING REMARKS

A number of techniques of X-rays, neutrons and others have been widely used for structural characterization of various materials. Each technique has, of course, its own advantages and disadvantages. However, as shown in this paper with some selected examples, the potential capability of the AXS method has been clearly demonstrated and this relatively new method is very promising for structural characterization of both crystalline and disordered materials by providing answers for questions unsolved by conventional techniques. For most of the elements, the change in the real component of the anomalous dispersion factor f' is typically $15 \sim 25\%$ of the normal atomic scattering factor f^0 at the K absorption edge and it appears to be a substantially larger value (over 50%) at the L absorption edge. Thus, the AXS method coupled with the intense white X-ray source (synchrotron radiation) is no longer a novel technique. It is rather one of the most reliable and powerful tools for structural characterization of various materials in a variety of states.

for High Energy Physics, Prof. M. Nomura and Dr. K. Koyama for their advise of AXS measurements.

REFERENCES

(1) Special issue of Anomalous X-ray scattering, *J. Cryst. Soc. Japan,* Vo. 19 (1977).

(2) Y. Waseda, Novel Application of Anomalous X-ray Scattering for Structural Characterization of Disordered Materials, Springer- Verlag, New York (1984).

(3) R.W. James, The Optical Principles of the Diffraction of X-rays, G.Bell & Sons, London (1954).

(4) P.A. Lee, P.H. Citrin, P. Eisenberger and B.M. Kincaid, *Rev. Mod. Phys.,* **53**, 61 (1981).

(5) B.K. Teo, EXAFS Basic Principles and Data Analysis, Springer-Verlag, Heiderberg (1986).

(6) S.Hosoya, *Rigaku Denki Journal,* **19**, 7 (1979).

(7) U. Bonse, I. Hartmann-Lotsch, H. Lotsch and K. Olthoff-Mienter, *Zeit. Physik,* **B47**, 297 (1982).

(8) D.T. Cromer and D. Liberman, *J. Chem. Phys.,* **53**, 1891 (1970).

(9) Y. Waseda, *IJIS Inter.,* **29**, 198 (1989).

(10) V.V. Rao, S.B. Reddy, G. Satyanarayana and D.L. Sastry, *Physica C,* **138**, 215 (1986).

(11) E. Matsubara, K. Harada, Y. Waseda and M. Iwase, *Z. Naturforsch.,* **43a**, 181 (1988).

(12) R.L. Mozzi and B.E. Warren, *J. Appl. Cryst.,* **2**, 164 (1969).

(13) K. Takahashi, N. Mochida, H. Matsui, S. Takeuchi and Y. Gohshi, *Yogyo-Kyokai-Shi (in Japanese),* **84**, 482 (1976).

(14) N. Mochida, T. Sekiya and A. Ohtsuka, *Yogyo-Kyokai-Shi (in Japanese),* **96**, 271 (1988).

(15) K.Q. Lu, Y.Q. Zhao, L.C. Chang, Z.J. Shen, W.W. Huang and Y.F. Lin, *Chinese Phys. Lett.,* **2**, 113 (1985).

(16) Y. Shimizugawa, C.D. Yin, M. Okuno, H. Morikawa, F. Marumo, Y. Udagawa, N. Mochida and T. Sekiya, *Yogyo-Kyokai-Shi (in Japanese),* **95**, 418 (1987).

(17) K. Sugiyama, Y. Waseda and M. Ashizuka, *Mater. Trans. JIM,* **32**, 1030 (1991).

(18) A.H. Narten, *J. Chem. Phys.,* **56**, 1905 (1972).

(19) A.H. Narten, F. Vaslow and H.A. Levy, *J. Chem. Phys.,* **58** , 5017 (1973).

(20) K. Sugiyama and E. Matsubara, *High Temp. Mater. Process,* **10**, 177 (1992).

(21) K.S. Mazdiyasni, C.T. Lynch and J. Smith, *J. Amer. Soc.,* **48**, 372 (1965).

(22) K.S. Mazdiyasni, C.T. Lynch and J. Smith, *J. Amer. Soc.,* **49**, 286 (1966).

(23) R.C. Garvie, *J. Phy. Chem.,* **69**, 1238(1965).

(24) Y. Murase, E. Kato and H. Matsumoto, *Nippon Kagaku Kaishi (in Japanese),* **12**, 2329 (1972).

(25) R. Cypres, R. Wollast and J. Raucq, *Ber. Dtsch. Keram .Ges.,* **40**, 527 (1963).

(26) A. Clearfield, *Inorg. Chem.,* **3**, 146 (1964).

(27) E.D. Whitney, *Trans. Fraday Soc.,* **61**, 1991 (1965).

(28) J. Livage, K. Doi, and C. Mazieres, *J. Amer. Cerm. Soc.,* **51**, 349 (1965).

(29) E. Tani, M. Yoshimura and S. Somiya, *J. Amer. Ceram. Soc.,* **66**, 11 (1983).

(30) K. Sugiyama, Y. Waseda and S. Kudo, *ISIJ Inter.,* **31**, 1362 (1991).

(31) J.D. McCullough and K.N. Trueblood, *Acta Cryst.,* **12**, 507 (1959).

(32) G. Teufer, *Acta Cryst.,* **15**, 1187 (1962).

(33) T. Sato, K. Haneda, M. Seki and T. Iijima, Proc. Inter. Symp. Physics of Magnetic Materials, World Scientific Pub., Singapore, p. 210 (1987).

(34) E. Matsubara, K. Okuda, Y. Waseda and T. Sato, *Zeit. fur Naturforsch.,* **47a**, 1023 (1992).

(35) B.E. Warren, X-ray Diffraction, Addison-Wesley Pub., Reading, Massachusetts (1969).

(36) F. Betts and A. Bienenstock, *J. Appl. Phys.,* **143**, 4591 (1972).

(37) Y. Waseda, E. Matsubara, K. Okuda, K. Omote, T. Tohji, S.N. Okuno and K. Inomata, *J. Phys. Condensed Matter,* **4**, 6355 (1992).